Editors' Suggestion

Detaching Microparticles from a Liquid Surface

Frank Schellenberger,[1] Periklis Papadopoulos,[2] Michael Kappl,[1] Stefan A. L. Weber,[1,3] Doris Vollmer,[1] and Hans-Jürgen Butt[1,*]

[1]Max Planck Institute for Polymer Research, Ackermannweg 10, 55128 Mainz, Germany
[2]University of Ioannina, Department of Physics, P.O. Box 1186, 45110 Ioannina, Greece
[3]Johannes Gutenberg University, Department of Physics, Staudingerweg 10, 55128 Mainz, Germany

(Received 23 February 2018; revised manuscript received 30 May 2018; published 27 July 2018)

The work required to detach microparticles from fluid interfaces depends on the shape of the liquid meniscus. However, measuring the capillary force on a single microparticle and simultaneously imaging the shape of the liquid meniscus has not yet been accomplished. To correlate force and shape, we combined a laser scanning confocal microscope with a colloidal probe setup. While moving a hydrophobic microsphere (radius 5–10 μm) in and out of a 2–5 μm thick glycerol film, we simultaneously measured the force and imaged the shape of the liquid meniscus. In this way we verified the fundamental equations [D. F. James, J. Fluid Mech. **63**, 657 (1974); A. D. Scheludko, A. D. Nikolov, Colloid Polymer Sci. **253**, 396 (1975)] that describe the adhesion of particles in flotation, deinking of paper, the stability of Pickering emulsions and particle-stabilized foams. Comparing experimental results with theory showed, however, that the receding contact angle has to be applied, which can be much lower than the static contact angle obtained right after jump in of the particle.

DOI: 10.1103/PhysRevLett.121.048002

Most micro- and nanoparticles spontaneously attach to liquid interfaces. Particle attachment and colloidal assembly at fluid interfaces [1–6] are of broad interest. For example, particles at fluid interfaces stabilize Pickering emulsions [7–10], foams [11,12], and liquid marbles [13–15]. The efficiency of mineral flotation or the deinking of paper is largely determined by the detachment probability of particles from bubble surfaces [16–18].

Since capillary forces are so relevant, they have been studied intensely, primarily with spherical particles as a model. When pulling a particle out of a liquid-fluid interface, a meniscus is formed which causes a retracting capillary force. This capillary force has been measured for millimeter-sized particles [16,19–21] down to 0.3 mm diameter [22]. Here, the size of the particle is comparable to the capillary length $\kappa = \sqrt{\gamma/\rho g}$; γ is the surface tension of the liquid, ρ is the density of the liquid, and $g = 9.81\ \mathrm{m/s^2}$ is the gravitational acceleration. For water, $\kappa = 2.7$ mm. Experiments with macroscopic spheres, where gravitation is usually significant, showed that the contact line slides over the surface at constant contact angle when the particle is retracted from the interface. Most applications are, however, concerned with microscopic particles. Size matters. For microparticles, where gravity is usually negligible as compared to capillary forces, the capillary force has not been experimentally correlated with the shape of a meniscus. So far capillary forces with microparticles have been measured using the colloidal probe technique for particle-bubble interaction [17,23–25], particles in thin liquid films [26–28] or at extended planar liquid-fluid interfaces [29–31]. In these measurements, however, the shape of the liquid-fluid interface remained unknown. In other experiments, microscopic menisci could be imaged, e.g., by environmental scanning electron microscopy [32–34] or confocal microscopy [35,36], but not correlated with a force. Therefore, many questions are still open: How are the shape of the meniscus and the capillary force related? Does the contact line slide over the particle surface or is it pinned when a force acts on the particle? The fact that we know little about the detachment of microparticles from interfaces is unfortunate, because particles with diameter below 100 μm are relevant for applications. In contrast to large particles, which are dominated by gravity and inertia, microparticles are dominated by capillary forces.

Here, we measured the force on individual microspheres and a liquid film versus distance using the colloidal probe technique. Simultaneously, the shape of the liquid meniscus was imaged by laser scanning confocal microscopy [Fig. 1(a)]. In this way we can quantitatively correlate the shape of the meniscus, the diameter of the contact line, and the capillary force for individual spherical microparticles.

In addition, we can compare observations to theory. Therefore, we give a brief outline of the fundamental theory. The capillary force acting on a sphere normal to a liquid-fluid interface is given by the direct action of the surface tension γ integrated around the three-phase contact line [37,38]:

$$F = 2\pi\gamma R \sin\beta \sin\alpha = 2\pi\gamma R \sin\beta \sin(\Theta + \beta). \quad (1)$$

Here, R is the radius, β describes the position of the three-phase contact line on the particle surface, Θ is the contact

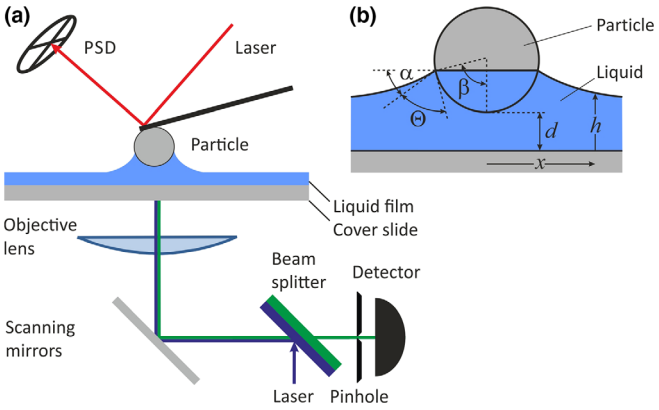

FIG. 1. (a) Schematic setup combining a colloidal probe setup with a confocal microscope. Position sensitive device (PSD). (b) Schematic of a particle in contact with a liquid film on a solid substrate.

angle, α is the angle of the liquid surface with the horizontal [Fig. 1(b)]. $R\sin\beta$ is the radius of the contact line. The angles are related by $\alpha = 180° - \beta - \Theta$.

Of particular relevance for most applications is the detachment force. The detachment force, also called adhesion force, is the force required to remove a particle out of the liquid-fluid interface. It is calculated by varying β in Eq. (1) at constant contact angle Θ. The maximal force is reached at $\beta_{\max} = (\pi - \Theta)/2$. Inserting $\beta_{\max}$ into Eq. (1) we obtain the detachment force of a sphere [38]:

$$F_{\max} = 2\pi\gamma R\cos^2\frac{\Theta_r}{2}. \tag{2}$$

The physical picture behind Eq. (2) is the following: When pulling on a sphere that is attached to a liquid-fluid interface a meniscus is formed and more and more stretched. While the meniscus extends, the contact line slides over the surface of the particle at constant contact angle Θ. β decreases and the capillary force increases until β reaches $(\pi - \Theta)/2$. Then the force decreases again. Finally, the liquid meniscus becomes unstable and ruptures. In Eq. (2) we take the receding contact angle Θ_r because when pulling the particle into the vapor phase, the contact line recedes over the particle surface. For millimeter sized spheres, Eqs. (1) and (2) have been confirmed experimentally [19,21,22,38,39]. The main aim of this work is to test if the theory and its main assumptions also hold for processes at length scales 2 orders of magnitude smaller.

To measure the force directly, spherical borosilicate glass particles (Duke Scientific Corp., radii 6–10 μm) were glued (Uhu Plus Endfest300, 2K Epoxy glue) to the end of rectangular, tipless silicon cantilevers (AppNano, SPM Probe ACL, spring constant $k_c = 36$–90 N/m) with the help of a micromanipulator (Narishige, MM0-203). For better reflectivity, the back sides of cantilevers were sputter coated with 2 nm Cr and 30 nm Au. Prior to adding the particle, we calibrated the spring constant with a reference cantilever (CLFC, Bruker AFM probes) on a JPK Nanowizard1. The particles on the cantilevers were hydrophobized by chemical vapor deposition for 1 h with (1H,1H,2H,2H)-perfluorooctyl trichlorosilane. Glass slides coated in a similar way showed advancing and receding contact angles with glycerol of $107 \pm 2°$ and $55 \pm 5°$, respectively, as measured with the sessile drop and a goniometer. To obtain force-displacement curves, the base of the cantilever was moved up and down at constant speed (0.3–1 μm/s) with the piezoelectric scanner of an Asylum MFP-1D ("dynamic case") or a JPK Nanowizard1 ("quasiequilibrium"). To convert force vs displacement to force-vs-tip sample-distance curves ("force curves"), the deflection of the cantilever was subtracted from the vertical piezo displacement by a custom LabView program or the JPK SPM data processing software.

The shape of the liquid film surface was imaged with a homemade inverted laser scanning confocal microscope (excitation laser wavelength: 473 nm, Cobolt Blue 25 mW) and an Olympus UPlanSApo $40\times/0.95$ dry objective. Two detectors simultaneously recorded the reflected and fluorescence light with a scanning frequency of 8000 lines/s. For scanning, the objective was vertically moved by a piezo stage underneath the sample to avoid affecting the force measurements. The resolution was <400 nm in the horizontal and <1 μm in the vertical direction.

As a liquid we chose glycerol (measured $\gamma = 0.0635$ N/m, refractive index $n = 1.47$, density $\rho = 1255$ kg/m^3 for our glycerol at 20 °C) to avoid evaporation (see Supplemental Material [40] for details). To form films, a dyed drop of a liquid mixture (1:1 vol % glycerol/ethanol + Alexa488 1 μg/mL) was deposited on glass slides (Carl Roth GmbH, 170 μm thick, 24×60 mm^2, cleaned with ethanol, followed by 3 min in an oxygen plasma cleaner). The liquid spread spontaneously. After evaporation of ethanol, a closed liquid film of 2–5 μm thickness has formed. We waited 12 h to exclude dewetting. Within this time, the glycerol film equilibrated with moisture from the surrounding air. The spherical particle on the cantilever was moved into the focus of the confocal microscope, above the film and within the range of the piezoelectric scanner. Vertical slices through the center of the particle were imaged with 4 images/s.

The reflection signal was used to identify the point of contact between microsphere and liquid. Fluorescence images were analyzed to obtain the shape of the liquid meniscus (Fig. S1 [40]). To locate the position of the liquid surface $h(x)$ at a given position x the fluorescence intensity along a column (vertical direction y) was fitted with $I = I_0/(1 + e^{(y-h)/b})$ after subtracting a low background intensity. Here, I_0 is the difference between the background intensity and the intensity in the liquid. b is the width of the intensity change. This procedure was repeated for every x in an image. Finally, every value for the local film thickness $h(x)$ was corrected by the refractive index $n = 1.47$. To extract R, a circle was fitted to the data points

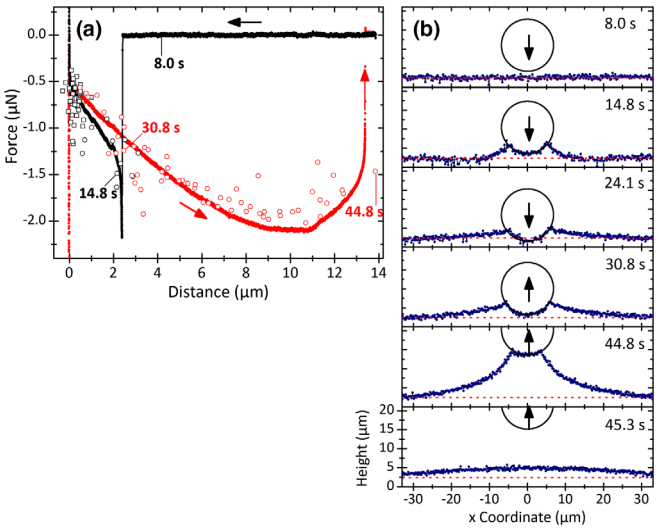

FIG. 2. (a) Representative force curve. A silica microsphere ($R = 6.9\ \mu$m, $k_c = 80.5$ N/m, approaching speed 0.5 μm/s) approached a film of glycerol of $h_0 = 2.5\ \mu$m thickness. Approaching (black) and retracting (red) parts are indicated by arrows. The open circles are forces calculated from the contact angle and contact line radius with Eq. (1). Positive forces are repulsive, negative forces attractive. (b) Shape of the liquid surface and the position of the particle from confocal microscopy images. The red dashed lines indicate the film thickness at large distance. The numbers indicate the time at which a specific force or profile was recorded.

representing the colloidal sphere. To extract the angles α, β, and Θ, the glycerol-air interface $h(x)$ was fitted in the range of 10–30 μm to the intersection with $h(r) = a_1 - a_2 \mathrm{arccosh}(r/a_3)$. This equation with fit parameters a_1, a_2, and a_3 in units of length solves the Laplace equation (see below) for zero gravity; it is a good approximation close to the particle. However, as we demonstrate below, the system is not in equilibrium and the equation only served to determine α, β, and Θ. At the intersection of the fitted circle and the fitted meniscus, α, β and the contact radii $R \sin\beta$ were calculated.

During large parts of the approach, the particle did not interact with the film and the force is zero [black symbols in Fig. 2(a)]. In the corresponding confocal microscope image, the flat, horizontal surface of the glycerol film was observed [Fig. 2(b), 8.0 s]. Then, a jump in was observed with a strong attractive force. Confocal microscope images verify that this jump in is correlated with the formation of a three-phase contact and a liquid meniscus [Fig. 2(b), 14.8 s]. Therefore, we attribute the jump to the action of capillary force, which pulls the particle downward. Around the meniscus, the film thickness slightly decreased since liquid is drawn into the meniscus depleting the film around it (Fig. S1 [40]). Such a transient depletion zone had been observed before [28]. After the initial jump, the capillary force decreased when the particle was moved further downwards [Fig. 2(b), 24.1 s]. During this movement, the contact line was pinned. The decrease in capillary force was correlated with a widening of the meniscus. Then the particle got into contact with the glass substrate and the distance was zero. While continuing to move the cantilever downwards the contact repulsion increased.

When retracting the cantilever again, at some point the particle overcame adhesion with the glass substrate [red symbols, Fig. 2(a)]. This is reflected by the pronounced negative force peak at zero distance. In this particular case, an adhesive force of 3.1 μN had to be overcome to release the particle from the glass; it is out of scale in Fig. 2(a). The adhesive force is the sum of contact adhesion plus a possible hydrodynamic contribution. Estimating contact adhesion with JKR theory [42], $F_{\mathrm{adh}} = 3\pi w R/2$, a work of adhesion of $w = 0.096$ N/m is obtained. This value is 2–3 times higher than reported values for even dry surfaces [43], indicating that also hydrodynamic forces hold the particle back. A further hint that hydrodynamic forces play a role is the observation that adhesion forces slightly increased with increasing retraction speed (Supplemental Material [40], Fig. S2).

After the particle was released from direct contact with the glass substrate, a broad meniscus was still dragging it down [Fig. 2(b), 30.8 s]. The capillary force monotonically increased until a distance of $\approx$10 μm was reached. Then it decreased until the meniscus ruptured at $d = 13.4\ \mu$m. Figure 2(b) (44.8 and 45.3 s) shows the shape of the liquid surface just before and after the meniscus ruptured. Immediately after the capillary bridge had broken, the liquid film was not flat, but slightly thicker in the center. This flat bump disappeared after several seconds due to the radial flow of glycerol.

To calculate the force, we inserted the angles measured by confocal microscopy into Eq. (1). The total force measured agreed with the force calculated from the shape of the liquid meniscus during the whole force cycle [filled and open red dots, respectively, Fig. 2(a)]. These results are the first direct experimental verification of Eq. (1) for microparticles.

The error of the direct force measurement is mainly due to imprecision in determining the spring constant; we determined it to be 11% (Supplemental Material [40]). The error in determining the capillary force from the shape of the meniscus by Eq. (1) can be estimated from error propagation:

$$\Delta F = 2\pi\gamma(\sin\beta \sin\alpha \Delta R + R \sin\alpha \cos\beta \Delta\beta + R \sin\beta \cos\alpha \Delta\alpha). \quad (3)$$

Here, ΔR, $\Delta\alpha$, and $\Delta\beta$ are the errors of the respective properties. From repeated measurements we estimate $\Delta R = 0.5\ \mu$m, $\Delta\alpha = \Delta\beta = 3°$. With typical values for R, α, and β the error is of the order of $\Delta F = 0.25\ \mu$N.

One of the key assumptions of the theory and Eq. (2) is that the contact line is free to slide over the particle surface. However, when moving the microparticle into the liquid

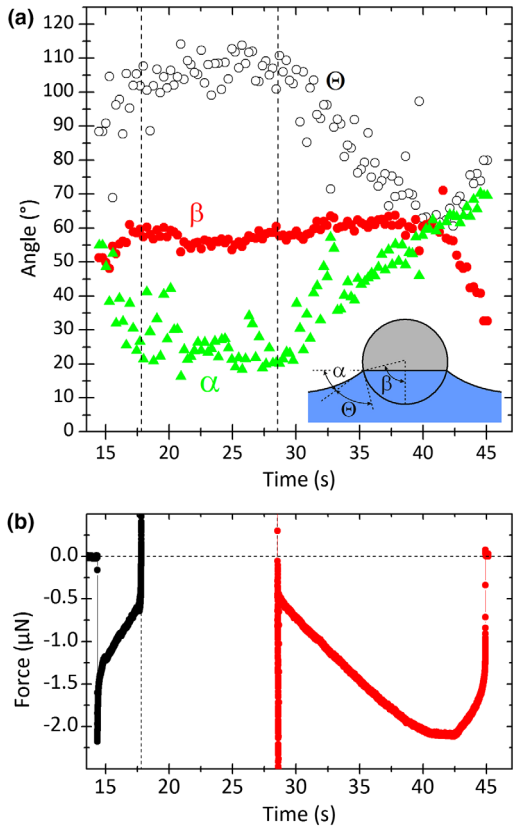

FIG. 3. (a) Position of the contact line (β, red), change of the contact angle (Θ, black), and angle of the liquid surface with the horizontal (α, green) during one representative force experiment. The three regimes of one force cycle are the free approach of the particle until 18 s, the contact of the particle with the glass substrate until 28 s and afterwards the retraction of the particle. For better comparison the same data as in Fig. 2 were used. (b) Measured force versus time with the approach (black) and retraction (red).

surface and retracting it again, the contact line was pinned during most of the process. Line pinning is demonstrated in Fig. 3(a) by plotting β versus time; a direct comparison with force vs time is shown in Fig. 3(b). For almost the whole force cycle, the contact line position is constant at $\beta \approx 60°$. In this respect, the retracting part, starting at $t = 27$ s, is most interesting: While β did not change and the contact line was pinned, the actual contact angle Θ decreased from 105° to 62°. At the same time, the angle α of the liquid meniscus with the horizontal increased from 25° to 60°. A change in capillary force is due to a changing contact angle Θ and α rather than a sliding contact line.

Only during the last few seconds ($t = 41$–45 s) the contact line was indeed sliding over the particle surface and β decreased. This final phase is characterized by a decreasing capillary force. In summary: Observations agree with the theory, if we assume a large contact angles hysteresis. The advancing contact angle of glycerol on the particle surface was $\Theta_a \geq 110°$, since 110° is the largest contact angle observed. As the receding contact angle, we take the measured contact angle just before the contact line starts sliding at $t = 41$ s. With a receding contact angle of $\Theta_r = 62°$ we calculate an adhesion force of 2.0 μN with Eq. (2). This value agrees with the measured value of $F_{\max} = 2.1$ μN. The maximum force should be reached at $\beta_{\max} = (\pi - \Theta)/2$. With $\Theta = 62°$, we calculate $\beta_{\max} = 59°$, which also agrees with the measured value. Thus, we observed a surprisingly high contact angle hysteresis. Taking this contact angle hysteresis into account, the observations on the microscale verify the commonly used theory of Scheludko [17,31,38,44].

One aim of this Letter is to relate the shape of the meniscus to its theoretical shape. Plots of the meniscus [Fig. 2(b)] demonstrate that the liquid is not in equilibrium but still flowing; see, for example, the local minimum in film thickness around $r = 15$ μm at 14.8 s and the central bump at 45.3 s (Fig. S3 [40]). To compare the imaged shape of the meniscus to its equilibrium shape given by the Young-Laplace equation, we needed to make sure that hydrodynamic flow in the film has subsided. Therefore, we approached and retracted the particle in steps of 1 μm. Between steps we waited for 60 min. Force measurements showed that indeed the force changed within the first 1–3 min after each step and saturated afterwards (Fig. S4 [40]).

In thermodynamic equilibrium, the shape of the liquid meniscus in the region around the particle is determined by the Young-Laplace equation [45,46]:

$$\frac{h}{\kappa^2} = \frac{h''}{(1+h'^2)^{3/2}} + \frac{h'}{r(1+h'^2)^{1/2}}. \tag{4}$$

Here, $h(r)$ is the height of the liquid film at a certain radial position r, $h' = dh/dr$, and $h'' = d^2h/dr^2$. For the full Young-Laplace equation, a general analytical solution is not available. However, the asymptotic regimes $r \ll \kappa$ and $r \gg \kappa$ can be solved and an analytical approximation can be obtained [46,47]. For the range of experimental observations ($r \ll \kappa$) and Bond numbers ($\mathrm{Bo} \equiv R/\kappa$) much lower than unity, a first order approximation describes the shape of the lubricant meniscus sufficiently good [46–49]:

$$h(r) = r_m \sin\alpha \left[\ln\left(\frac{4\kappa}{r + \sqrt{r^2 - r_m^2 \sin^2\alpha}} \right) - 0.577 \right] + b. \tag{5}$$

Here, $r_m = R \sin\beta$ is the radius of the contact line and 0.577 is the Euler-Mascheroni constant. In our experiments $\mathrm{Bo} \approx 0.003$ so that Eq. (5) can be applied. Note that Eq. (5) diverges for large r. Therefore, when fitting experimental results with Eq. (5) the constant b was added. b has, however, no intuitive physical meaning.

The liquid menisci 59 min after a step could indeed be fitted with Eq. (5) (black symbols, Fig. S5 [40]). In contrast, shapes recorded at a constant retraction speed, as shown in Fig. 2, could not be fitted with Eq. (5) (red

symbol, Fig. S5 [40]). With respect to applications it is important to note that the observed slow dynamics is due to the low thickness of the solid supported glycerol film and the high viscosity. No such slow relaxation is expected in flotation, in foams, or emulsion films.

In conclusion, using confocal microscopy we could simultaneously image the shape of the liquid meniscus and measure the capillary force acting on a microsphere attached to a liquid surface. We verified that Eq. (1) indeed describes the capillary force for micrometer-sized spherical particles. The adhesion force can be calculated with Eq. (2) assuming a large contact angle hysteresis between advancing and receding contact angles. The receding contact angle has to be inserted into Eq. (2). One should be aware that the receding contact angle can be much lower than the contact angle obtained after jump in. When the system is in quasiequilibrium, the shape of a liquid meniscus around a colloidal particle is described by the theory of James [Eq. (5)].

The data obtained and analyzed that support the findings of this study are available upon reasonable request.

We acknowledge financial support from ERC Advanced Grant No. SuPro 340391 (H.-J. B.), technical support by Uwe Rietzler and stimulating discussions with Tadashi Kajiya and Ansgar Schäfer. We further thank Janet A. W. Elliott and Nadia Shardt, University of Alberta, for providing us data on glycerol-water mixtures.

F. S. assembled the confocal microscope, conducted the experiments and analyzed the images. P. P. helped in setting up the confocal microscope and analyzing the images. M. K. and S. W. helped in the colloidal probe experiments. H.-J. B. devised and supervised the study and had the initiative in preparing the manuscript. D. V. and everybody else helped interpreting the results and preparing the manuscript.

*butt@mpip-mainz.mpg.de

[1] P. Pieranski, Phys. Rev. Lett. **45**, 569 (1980).
[2] N. D. Denkov, O. D. Velev, P. A. Kralchevsky, I. B. Ivanov, H. Yoshimura, and K. Nagayama, Nature (London) **361**, 26 (1993).
[3] F. Bresme and M. Oettel, J. Phys. Condens. Matter **19**, 413101 (2007).
[4] M. E. Cates and P. S. Clegg, Soft Matter **4**, 2132 (2008).
[5] L. C. Bradley, W. H. Chen, K. J. Stebe, and D. Lee, Curr. Opin. Colloid Interface Sci. **30**, 25 (2017).
[6] S. Dasgupta, T. Auth, and G. Gompper, J. Phys. Condens. Matter **29**, 373003 (2017).
[7] R. Aveyard, B. P. Binks, and J. H. Clint, Adv. Colloid Interface Sci. **100–102**, 503 (2003).
[8] T. N. Hunter, R. J. Pugh, G. V. Franks, and G. J. Jameson, Adv. Colloid Interface Sci. **137**, 57 (2008).
[9] S. Lam, K. P. Velikov, and O. D. Velev, Curr. Opin. Colloid Interface Sci. **19**, 490 (2014).
[10] M. Zanini, C. Marschelke, S. E. Anachkov, E. Marini, A. Synytska, and L. Isa, Nat. Commun. **8**, 15701 (2017).
[11] A. R. Studart, U. T. Gonzenbach, I. Akartuna, E. Tervoort, and L. J. Gaukler, J. Mater. Chem. **17**, 3283 (2007).
[12] F. Gorlier, Y. Khidas, and O. Pitois, Soft Matter **13**, 4533 (2017).
[13] P. Aussillous and D. Quéré, Nature (London) **411**, 924 (2001).
[14] G. McHale and M. I. Newton, Soft Matter **7**, 5473 (2011).
[15] M. Paven, H. Mayama, T. Sekido, H.-J. Butt, Y. Nakamura, and S. Fujii, Adv. Funct. Mater. **26**, 3199 (2016).
[16] D. X. Feng and A. V. Nguyen, Adv. Colloid Interface Sci. **248**, 69 (2017).
[17] Y. W. Xing, X. H. Gui, L. Pan, B. E. Pinchasik, Y. J. Cao, J. T. Liu, M. Kappl, and H. J. Butt, Adv. Colloid Interface Sci. **246**, 105 (2017).
[18] G. Suaria, C. G. Avio, A. Mineo, G. L. Lattin, M. G. Magaldi, G. Belmonte, C. J. Moore, F. Regoli, and S. Aliani, Sci. Rep. **6**, 37551 (2016).
[19] C. Huh and S. G. Mason, Can. J. Chem. **54**, 969 (1976).
[20] D. N. Mazzone, G. I. Tardos, and R. Pfeffer, J. Colloid Interface Sci. **113**, 544 (1986).
[21] E. Bayramli and T. G. M. Van de Ven, J. Colloid Interface Sci. **116**, 503 (1987).
[22] O. Pitois and X. Chateau, Langmuir **18**, 9751 (2002).
[23] H.-J. Butt, J. Colloid Interface Sci. **166**, 109 (1994).
[24] W. A. Ducker, Z. Xu, and J. N. Israelachvili, Langmuir **10**, 3279 (1994).
[25] R. F. Tabor, R. Manica, D. Y. C. Chan, F. Grieser, and R. R. Dagastine, Phys. Rev. Lett. **106**, 064501 (2011).
[26] M. M. Yazdanpanah, M. Hosseini, S. Pabba, S. M. Berry, V. V. Dobrokhotov, A. Safir, R. S. Keynton, and R. W. Cohn, Langmuir **24**, 13753 (2008).
[27] A. P. Bowles, Y. T. Hsia, P. M. Jones, L. R. White, and J. W. Schneider, Langmuir **25**, 2101 (2009).
[28] J. Ally, E. Vittorias, A. Amirfazli, M. Kappl, E. Bonaccurso, C. E. McNamee, and H. J. Butt, Langmuir **26**, 11797 (2010).
[29] C. E. McNamee, M. Kappl, H. J. Butt, K. Higashitani, and K. Graf, Langmuir **26**, 14574 (2010).
[30] L. Q. Chen, L. O. Heim, D. S. Golovko, and E. Bonaccurso, Appl. Phys. Lett. **101**, 031601 (2012).
[31] S. E. Anachkov, I. Lesov, M. Zanini, P. A. Kralchevsky, N. D. Denkov, and L. Isa, Soft Matter **12**, 7632 (2016).
[32] M. Schenk, M. Füting, and R. Reichelt, J. Appl. Phys. **84**, 4880 (1998).
[33] B. L. Weeks, M. W. Vaughn, and J. J. DeYoreo, Langmuir **21**, 8096 (2005).
[34] S. D. N. Lourenco, D. Gallipoli, C. E. Augarde, D. G. Toll, P. C. Fisher, and A. Congreve, Géotechnique **62**, 193 (2012).
[35] C. Gögelein, M. Brinkmann, M. Schröter, and S. Herminghaus, Langmuir **26**, 17184 (2010).
[36] F. Bossler and E. Koos, Langmuir **32**, 1489 (2016).
[37] G. D. Yarnold, Proc. Phys. Soc. London **58**, 120 (1946).
[38] A. D. Scheludko and A. D. Nikolov, Colloid Polymer Sci. **253**, 396 (1975).
[39] D. N. Mazzone, G. I. Tardos, and R. Pfeffer, Powder Technol. **51**, 71 (1987).

[40] See Supplemental Material at http://link.aps.org/supplemental/10.1103/PhysRevLett.121.048002 for details of cantilever calibration, image analysis, and further figures, which includes Ref. [41].
[41] C. T. Gibson, G. S. Watson, and S. Myhra, Nanotechnology **7**, 259 (1996).
[42] K. L. Johnson, K. Kendall, and A. D. Roberts, Proc. R. Soc. A **324**, 301 (1971).
[43] L. O. Heim, J. Blum, M. Preuss, and H.-J. Butt, Phys. Rev. Lett. **83**, 3328 (1999).
[44] A. V. Nguyen and H. J. Schulze, *Colloidal Science of Flotation*, Surfactant Science Series 118 (Marcel Dekker, Inc., New York, 2003).
[45] N. L. Cross and R. G. Picknett, Trans. Faraday Soc. **59**, 846 (1963).
[46] D. F. James, J. Fluid Mech. **63**, 657 (1974).
[47] B. V. Derjaguin, Dokl. Akad. Nauk SSSR **51**, 517 (1946).
[48] L. L. Lo, J. Fluid Mech. **132**, 65 (1983).
[49] P. A. Kralchevsky, I. B. Ivanov, and A. D. Nikolov, J. Colloid Interface Sci. **112**, 108 (1986).